Microfluidic Study of Foams Flow for Enhanced Oil Recovery (EOR).

N. Quennouz, M. Ryba, Jean-François Argillier, Benjamin Herzhaft, Yannick Peysson, Nicolas Pannacci

Oil & Gas Science and Technology – Rev. IFP Energies nouvelles, Vol. 69 (2014), No. 3, pp. 457-466

DOI: 10.2516/ogst/2014017

IFP Energies nouvelles International Conference
Rencontres Scientifiques d'IFP Energies nouvelles

Colloids 2012 - Colloids and Complex Fluids: Challenges and Opportunities
Colloids 2012 - Colloïdes et fluides complexes : défis et opportunités

Microfluidic Study of Foams Flow for Enhanced Oil Recovery (EOR)

N. Quennouz, M. Ryba, J.-F. Argillier, B. Herzhaft, Y. Peysson and N. Pannacci*

IFP Energies nouvelles, 1-4 avenue de Bois-Préau, 92852 Rueil-Malmaison Cedex - France
e-mail: nicolas.pannacci@ifpen.fr

* Corresponding author

Résumé — **Étude en microfluidique de l'écoulement de mousses pour la récupération assistée** — Cet article présente, dans le cadre de la récupération assistée du pétrole (EOR *Enhanced Oil Recovery*), une étude expérimentale avec des dispositifs microfluidiques concernant les écoulements de mousse dans des canaux de différentes géométries. Deux processus différents de formation de mousse ont été étudiés. Le premier correspond à la co-injection de gaz et d'eau à travers une jonction en croix produisant une mousse monodisperse. Le second correspond à la fragmentation de grosses bulles par un milieu poreux, processus de formation de mousse simulant des écoulements multiphasiques dans des roches. La formation de mousse est contrôlée et caractérisée en variant les pressions appliquées d'eau et de gaz. Nous avons également utilisé un microsystème avec deux perméabilités permettant la mise en évidence de la redirection de la phase continue vers les canaux de faible perméabilité. Ces observations sont importantes pour une meilleure compréhension des phénomènes impliqués dans les processus EOR ainsi que pour déterminer les données d'entrée pertinentes pour les simulateurs d'écoulement.

Abstract — ***Microfluidic Study of Foams Flow for Enhanced Oil Recovery (EOR)*** — *In this paper, we report an experimental study of foam flow in different channel geometries using microfluidic devices in the framework of EOR (Enhanced Oil Recovery). Two different processes of foam formation are studied. The first one corresponds to co-injection of gas and water through a cross junction which gives rise to a monodisperse foam. The second one corresponds to the fragmentation of large bubbles by a porous media, a foam formation process simulating multiphase flows in rocks. The foam formation is completely controlled and characterized varying both the water and gas pressure applied. We also use a microdevice with two permeabilities that permits to highlight the diversion of the continuous phase in the low permeability channels. The observations are important for a better understanding of the implied phenomena in EOR as well as to determine pertinent data to feed flow simulators.*

INTRODUCTION

Liquid foams are dispersions of bubbles of gas in a liquid continuous phase. They are widely used in several applications. Understanding and control of foam flow are issues for numerous processes and have been the subject of a lot of studies in EOR context [1-8]. In the framework of porous media, the foam's definition is more ambiguous as foam is composed mainly of thin liquid films known as lamellae. The lamellae are stabilized by the presence of surfactant at the gas/liquid interfaces. Because foam has an effective viscosity much higher than that of gas, it has been investigated as a method for improving sweep efficiency in processes where gases (such N_2, CO_2, steam, or hydrocarbon rich flue gas) are injected to improve oil recovery from mature reservoirs. Foam can reduce viscous fingering and gravity override caused by the low viscosity and density of the gas. Moreover, since fluids flow preferentially into layers of high permeability in an heterogeneous formation, foam will be preferentially formed in these high permeability zones and will greatly increase local resistance to flow, thereby diverting injected fluids to zones of lower permeability and improving process efficiency. Foam could therefore be used advantageously for EOR in fractured rocks, where great difficulties are encountered to contact EOR products like surfactant with the porous matrix because the flow takes place mainly in the fractures network (permeabilities in the fractures are much greater than the permeability of the rock matrix). Recent lab experiments by Haugen *et al.* [9] have shown that in a fractured carbonate, injection of foam allows an oil recovery up to 78% of the Original Oil In Place (OOIP), while oil recovery with only waterflooding is less than 10% (OOIP). Foam has diverted at least some of the displacing fluid into parts of the rock that were previously unswept or underswept.

In field conditions, there are two main techniques to obtain foam in porous media: co-injection of gas and aqueous surfactant or alternating injection of surfactant and gas. The choice of the injection strategy depends mostly on reservoir properties like permeability, wettability and their heterogeneities. In general, the gas volume fraction is very high, and we talk about dry foam, also called strong foam in the oil industry. Foam confined in a pore network has a morphology different from that of bulk foam [10]. So, bulk foam properties should therefore be compared to confined foam with caution. To guarantee the success of a foam EOR process, it is of great importance to be able to describe and model correctly the stability (like in presence of oil) and the transport of foam in porous media, from microscopic-scale to reservoir-scale. Although important advances in this field have been made [4, 5], there is still a need of detailed information on the physical mechanisms that control the structure, stability and mobility of the foam at the pore level.

The use of microfluidic devices is an interesting way to get better insight of these phenomena at small scale with the objective of a detailed physical description. Two decades ago fast prototyping was described to permit fabrication of channels in polymer with a typical dimension of hundred micrometers. Such a technique named "microfluidics" was then developed and used in very different domains (physical chemistry, biology, drug delivery, etc.), when flow control at the micrometric scale is an issue. Microfluidics appeared quickly as a good opportunity to study confined gaseous dispersed phases because of the high control on bubble formation and consequently on foam type. Studies in a such way by Marmottant and Raven [11], Marchalot *et al.* [12] and Ma *et al.* [13] have been done in the recent years.

We present here a study concerning the use of microfluidic geometries to analyse with simplified systems the formation, the flow and morphology description of confined foam in channels of different sizes. We quantify phase diagram of foam, conditions of foam formation and report new observations on the flow of bubbles in a comb geometry characterized by a dual permeability of channels mimicking fractured reservoir.

1 MATERIALS AND EXPERIMENTS

Microfabrication was done using standard soft lithography in PDMS (PolyDimethylSiloxane, *Sylgard*) such as described by Duffy *et al.* [14]. Such a fabrication produces a quasi-2D device with the same depth everywhere (typically 40 μm). In main cases, PDMS channels internal surface was hydrophilic due to bonding (PDMS on glass) with a plasma cleaner [15], such a surface treatment maintains water as the phase in contact with the internal walls of the microdevice. As this treatment is not stable in time (it lasts of the order of few hours), the microfluidic device was regularly renewed in order to keep the same surface properties for each experiment. As shown in Figure 1, the microfluidic devices used are composed of two entrances for gas and fluid, a simple cross junction where bubbles are formed, a chamber for the foam observation and downstream are three channels with different widths to connect the chamber to the outside (atmospheric pressure). Fluid and gas flows are obtained applying entrance pressure above atmospheric pressure (MFCS^{TM} 4C 1000 mbar, *Fluigent*) and constant flow rate in time was reached before any measurement. When necessary, flow rate of the

aqueous phase was measured thanks to a flowmeter (FLOWELL™, *Fluigent*). Gas flow rate in the channel is deduced from bubble trajectories in the gas stream with image analysis, with the assumption that the observed section of the bubble is constant in the channel depth (the calculated bubble volume is the one of a cylinder of height equal to the depth of the channel for a circular section). Flow observations were done thanks to a fast camera (fps 800) with optical microscopy. Gas used in this study is nitrogen and the water phase is composed of distilled water and SDS (Sodium *n*-dodecyl sulfate, *Alfa Aesar*®) surfactant at 1% w/w. In some experiments we dye the solution with methylene blue to improve the image analysis.

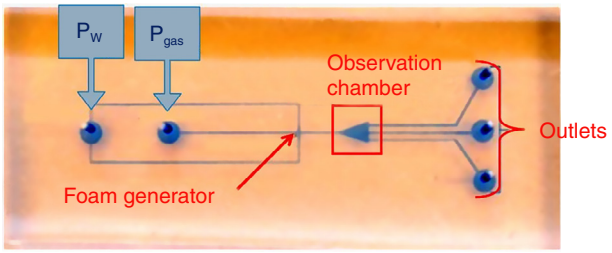

Figure 1

Microfluidic device: from left to right: water and gas entrance, bubble generator, collector and downstream channels. Scale: width of the channels is 60 µm. Channels are filled with oil containing organol blue for visualisation.

2 PHASE DIAGRAM AS A FUNCTION OF WATER AND GAS PRESSURE

We first performed a phase diagram to study the morphology of the foam according to water and gas pressures applied (*Fig. 2*). In this study, we impose the gas and the liquid pressure at entrance instead of the flowrate. The gas and water mixing is obtained at

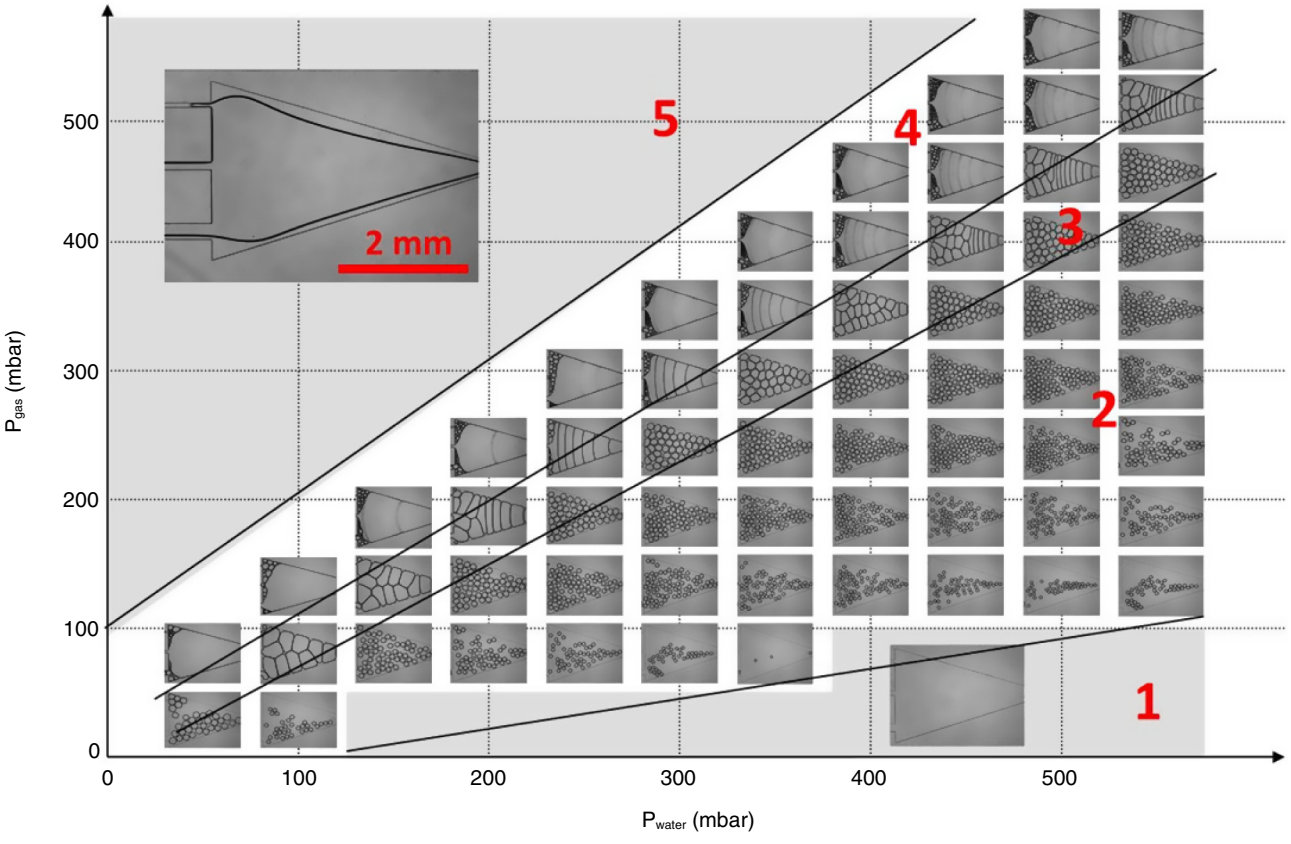

Figure 2

Diagram of foam formation in a confined medium according to the injection conditions (water pressure and gas pressure).

flow-focusing geometry (main channels section is 60 µm × 40 µm) and observed downstream in a triangular chamber (chamber axes are 1.4 mm × 2 mm) to have a larger zone of observation. A very large domain of foam quality is accessible (bubbly liquid with gas volumic fraction < 5% to dry foams with gas fraction > 90%). Micrometric to millimetric apparent bubbles diameter can be observed. Similarly to the phase diagram obtained by Raven *et al.* [16] we can notice five regions: for low applied gas pressure, only water is present in the observation chamber (region 1). When increasing gas pressure, small independent bubbles are formed and transported (region 2). In a third region, bubbles begin to touch and deform to polyhedral shapes, progressively leading to a foam composed of lamellae (region 4). At high gas pressure (region 5), a continuous gas flow is observed with residual water without any foam structure.

To describe the limit shown in Figure 2 between region 1 and 2 at low gas pressure, we measured experimentally the minimum pressure to apply to the gas phase P_{gas} for a given water pressure P_{water} to form a single bubble. Notice that we name P_{gas} and P_{water} the pressure difference with atmospheric pressure P_0. The values obtained experimentally are reported in Figure 3 for water only and water + SDS. We calculated analytically the minimum pressure needed to form the first bubble. Let us write that the applied pressure gap at the interface should exceed the Laplace pressure in the following case: a static non wetting bubble confined in a channel of width w and depth d with a surface tension γ. We take into account wetting behaviour through the wetting angle θ, defined as the angle between two planes intersecting at the triple line PDMS-Gas-Water and tangent respectively to the water-gas and to the water-PDMS interfaces:

$$\Delta P = Pi_{gas} - Pi_{water} = 2\gamma\left(\frac{1}{w}+\frac{1}{d}\right)\cos(\theta) \qquad (1)$$

where Pi_{gas} and Pi_{water} are respectively the gas and water pressure on both sides of the interface and at the cross junction.

Concerning gas, we can assume that pressure losses in the microchannels are negligible since gas viscosity is hundred time smaller that the one of water:

$$Pi_{gas} = P_{gas} + P_0 \qquad (2)$$

Concerning water at a flow rate Q, taking into account that pressure losses are the sum of the hydraulic resistances upstream and downstream the bubble formation zone, respectively R_u and R_d, we have:

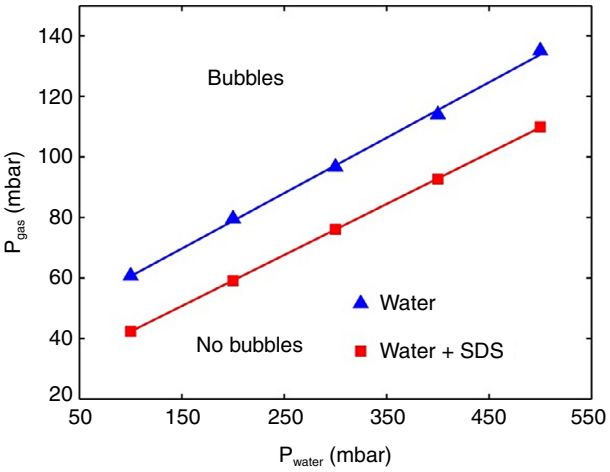

Figure 3

Bubble formation limit according to water and gas pressures applied. Effect of change of surface tension due to surfactant is shown (with or without SDS) and for a hydrophilic surface treated PDMS.

$$P_{\text{water}} = Q(R_{\text{u}} + R_{\text{d}}) \qquad (3)$$

and

$$Pi_{\text{water}} = P_0 + QR_{\text{d}} \qquad (4)$$

leading to:

$$P_{gas} = 2\gamma\left(\frac{1}{w}+\frac{1}{d}\right)\cos(\theta) + \frac{R_d}{R_u+R_d}P_{water} \qquad (5)$$

This model shows a linear relationship between P_{water} and P_{gas} with a threshold. The gas pressure has to overcome a certain value to create a bubble. The experimental measurements have the same trend. To go a little further, we compare the value of the surface tension obtained by this model to the one measured thanks to Wilhelmy plate method for distilled water with 1% SDS: $\gamma = 30.8 \pm 0.1$ mN/m. For this we fit the experimental data by a linear function (red solid line of *Fig. 3*) and we deduce from the y-intercept and Equation (5) the value of γ knowing w and d. Experimentally, complete wetting of water and surfactant on channel's walls is obtained in case of hydrophilic PDMS, so $\cos(\theta) = 1$. With this model we find a surface tension of 31.2 ± 0.3 mN/m in very good agreement with the Wilhelmy plate measurement. We do the same for data obtain with distilled water and we obtain for our model

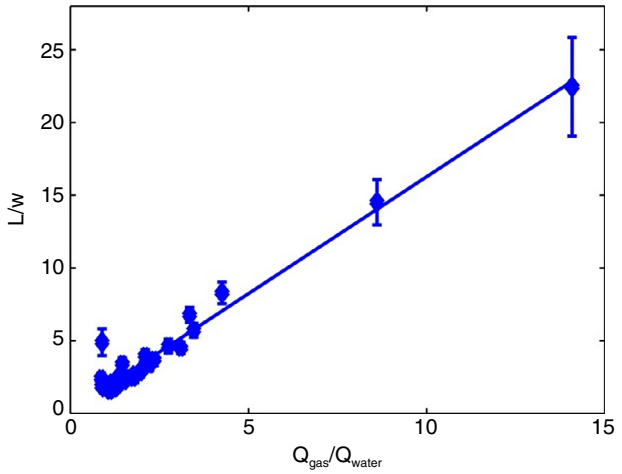

Figure 4

Characteristics of bubble formation: relative size as function of relative flow rates.

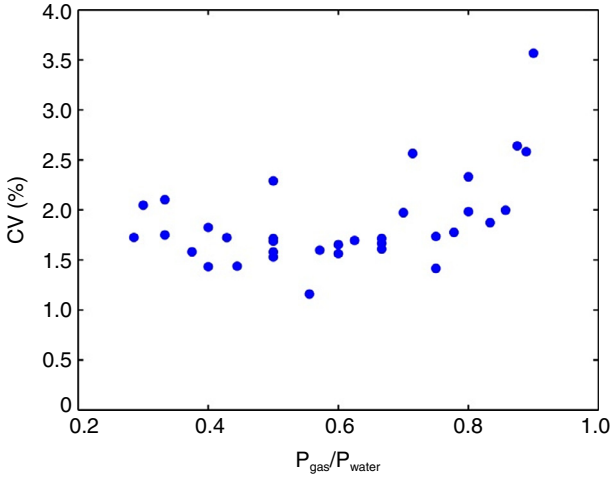

Figure 5

Coefficient of variation of the bubbles observed in the chamber.

$\gamma = 50.7 \pm 0.3$ mN/m. The difference observed between this value and the tabulated surface tension [17] of distilled water ($\gamma = 72$ mN/m) can be explained by a pollution of the water during its flow in the connectors and the channel and by a partial wetting of the water. For this kind of experiments, microfluidic devices allow the realisation of large number of measurement in very short time (we observe about 100 bubbles during few minutes) so an easy reduction of statistical uncertainty can be obtained.

3 FOAM CHARACTERIZATION

Thanks to image analysis, the bubble structure in the foam was also characterized.

Measurements shown in Figure 4 are obtained in the case of an imposed flow rate for the water phase, with a variation of the pressure applied to the gas phase. Applied flow rates for water were varied between 2.5 and 15 μL/min and gas pressure from 40 to 500 mbar with 50 mbar steps. Image analysis allows measurement of the apparent area of the bubbles from which we can deduce the length of the bubbles formed at the junction. The variation of the length of the bubble formed compared to the width of the channel is found to be linear, in agreement with the model developed by Garstecki *et al.* [18] for a T-junction:

$$\frac{l}{w} = \alpha\left(Q_g/Q_l\right)^{\beta} \tag{6}$$

We have, after adjustment of this model to our experimental data the linear behaviour:

$$\frac{l}{w} = 1.77\frac{Q_g}{Q_l} \tag{7}$$

Other model confirms the order of magnitude of α in case of a flow-focusing geometry [19].

Figure 5 presents the Coefficient of Variation (CV) of the bubbles sizes observed in the chamber when both gas and water pressures were varied between 0 and 500 mbar. CV is calculated as the ratio of the standard deviation of the apparent diameter of a sample of bubbles to the mean bubble apparent diameter for a given gas pressure and a given water pressure measured. The samples considered are in the order of a hundred of bubbles. With the flow focusing device bubbles formed are particularly monodisperse, with CV equal to 1.5-2% as already shown in the litterature. For instance Stoffel *et al.* [20] formed bubbles with CV < 1%. As a comparison, standard bulk emulsification processes give raise to CV of 15% [21]. One simple explanation of such a small polydispersity is that bubbles are formed one by one in a quasistationnary flow regime.

In Figure 6 is represented the increase of the gas volume fraction *i.e.* the quality of the foam for gas pressure and water pressure varying on the range 0-500 mbar, as in the phase diagram. To measure the foam quality we calculated the ratio between the area occupied by the gas and the area occupied by the liquid. These areas are measured thanks to an image analysis

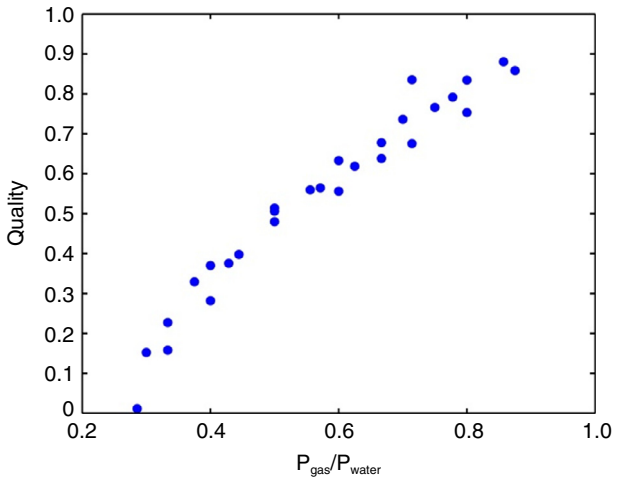

Figure 6

Quality of the foam (the gas volume fraction) for different gas/water injection conditions.

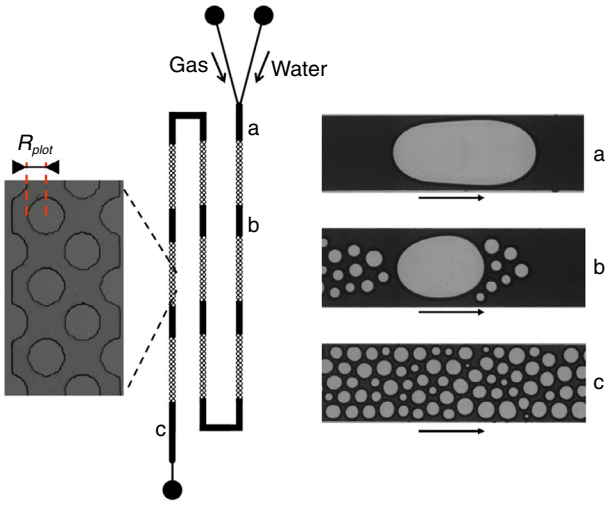

Figure 7

On the left: geometry used for the foam formation by a porous media. On the right: snapshots of bubbles flow is from the left to the right: a) just after the "Y" junction, b) after one matrice of plot crossed, c) after 9 matrices.

(Matlab software). To differentiate the gas from the liquid we took advantage of the contrast difference between the two phases. The quality is shown to follow a master curve when drawn as a function of the gas to water pressure ratio.

4 FOAM FLOW IN A POROUS MEDIA

In the previous part we have characterized the foam obtained by co-injection of gas and water thanks to a cross junction. Now, we study the foam formation issued from the fragmentation of a large initial bubble by an assembly of obstacles. This kind of fragmentation was previously studied by Protière *et al.* [22] where they focused on droplet breakup by a single obstacle and studied the influence of the capillary number on the fragmentation. For this study, we use a micro device (*Fig. 7*) constituted of a "Y" junction in order to form initially very large bubbles by injecting gas and water in the two entrances and 9 matrices of plot (R_{plot} = 90 ± 4 µm and the smaller distance between two plots is 56 ± 4 µm) with a length equal to 5 mm. The channel section is 500 ± 4 µm × 47 ± 2 µm. For the outlets we simply use holes in PDMS of 4 mm in diameter allowing flows to end at atmospheric pressure, with negligible hydraulic resistance. The matrices are separated by observation chamber in order to evaluate the influence of the total porous media length crossed called L_p. In Figure 8, we represent the ratio between the mean equivalent radius of the fragmented bubbles

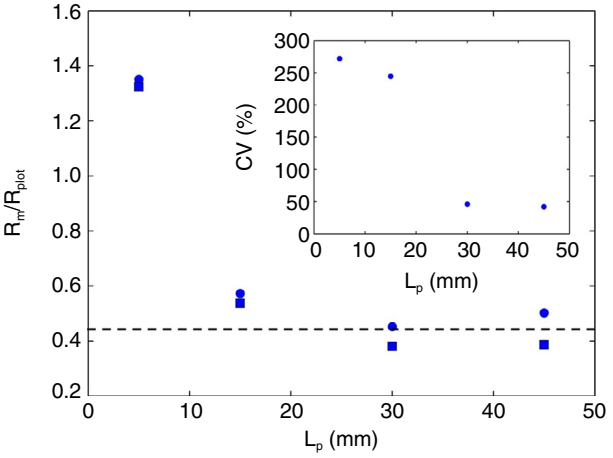

Figure 8

Normalized radius of the bubbles as a function of L_p for P_{gas}/P_{water} = 0.8. Circles correspond to the observed radius of bubbles and squares correspond to data with the correction taking into account pressure losses. Insert shows the dispersion of the bubbles area as a function of L_p.

R_m and the radius of the plot R_{plot} as a function of L_p for P_{gas}/P_{water} = 0.8.

R_m is obtained by measuring the areas of the bubbles from which we deduce the bubbles size distribution. We calculate an average radius of the fragmented bubbles, taking into account 200 large initial bubbles.

For lisibility reasons we do not represent the data for the bubbles just after their formation by the "Y" junction (corresponding to the snapshot of *Fig. 7a*). This graph shows that the mean radius of the fragmented bubbles decreases with the crossed length of the porous media for $L_p < 20$ mm, then stabilizes around $R_m/R_{plot} = 0.44$ which corresponds to a mean radius of bubble $R_m = 40$ µm. We notice that R_m and the smaller distance between two plots have the same order of magnitude. If we observe carefully the data (circle) we can notice a slight increase of R_m/R_{plot} for large values of L_p. This increase is attributed to the pressure losses in the microchannel as the pressure goes down, the bubble volume rises. Squares represent R_m/R_{plot} taking into account pressure losses. For this correction, we consider in first approximation the pressure losses in a channel without plot and a Newtonian fluid (using the calculation:

$$R_{corr}(L_p) = \left(\sqrt{1 - \frac{P_{water}}{P_0 + P_{water}}\frac{L_p}{L_{tot}}}\right) R_{obs}(L_p)$$

where R_{corr} and R_{obs} correspond respectively to the corrected and the observed radius at the position L_p and L_{tot} the total length of the channel. P_0 is the atmospheric pressure and P_{water} the pressure of the injected water). Taking into account these pressure losses, the increase of the mean radius are no more observed for large value of L_p. The measurement uncertainty of R_m is about 4 µm.

In the insert of Figure 8 is plotted the coefficient of variation of the fragmented bubbles areas. The coefficient of variation of foam formation by fragmentation decreases with L_p until $L_p = 30$ mm where it reaches a stable value of 50%. We notice that the foam formation by fragmentation mechanism by a porous media leads to a much more important polydispersity of the bubbles compared to the mechanism using co-injection through a cross junction (*Sect. 2*). We did the same analysis for five other values of P_{gas}/P_{water} and the results show the same trend. Here, we highlight the influence of the length of the porous media on the bubbles size and an other study [23] showed that the viscosity of the liquid is a critical parameter determining the bubble size.

5 FLOW IN A COMB: TWO PERMEABILITIES MODEL

Foam flow in porous media can be very important for the petroleum industry. Indeed, for the specific case of fractured reservoirs, the classical methods of oil recovery like water flooding or chemical injection are inefficient because the low permeability porous matrix is not swept due to the very large permeability contrast between fractures and matrix. In 1961, a first experiment of foam injection in porous natural rock was made by Fried [24]. It has been shown latter in the literature that foam can also enhance flow diversion in heterogeneous media [25, 26].

In order to better understand the flow of foam in a heterogeneous medium we have performed experiments using a comb-like micro-model with two "permeabilities". A related experiment was already conducted by Prat *et al.* [27] who looked at the diversion of the continuous phase in lateral channels using microfluidic devices in order to control the distance between droplets in a droplet train.

As shown in Figure 9 our microfluidic device comprises from right to left: water, gas entrance and foam generator with the same geometry as the device shown in Figure 1 and described above producing an initial foam with a quality between 0.1 to 0.9. Downstream is a large channel of 300 µm in width with orthogonal narrow channels of 20 µm in width and 40 µm in height. On the left outlets are holes in PDMS of 4 mm in diameter. Such a "comb" may mimic in a simplified way a fractured reservoir.

First observations show that when flow begins, small channels allow only water flows, resulting in a progressively drying of the foam in the main channel. After a certain period of time (5 s), a stationary state is obtained, characterized by the relative slow-down of the biphasic flow in the large channel and the redirection of the dispersion through the small channels (*Fig. 10*). Indeed, we observe that bubbles can enter and flow in the lateral channels. We can also observe fragmentation of bubbles when they pass close to the entrance of the small lateral channels, and the small bubbles can then flow in it. We note that the bubbles enter mainly in the first lateral channels. To go further in the understanding of the foam

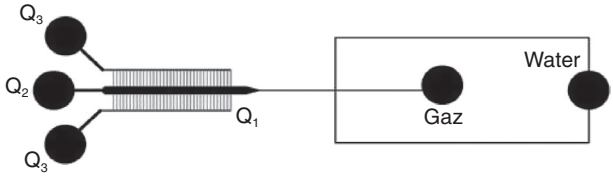

Figure 9

Geometry used in the two permeabilities comb-type experiment. Length is about 2 cm. Parts in dark correspond to the channels, see text for details.

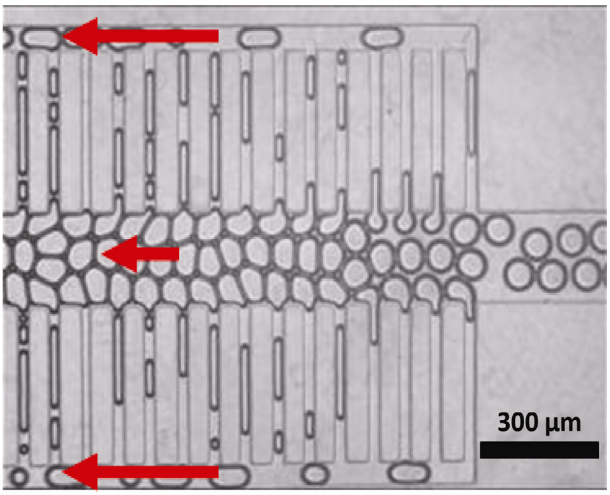

Figure 10

Diversion of the flow due to bubble accumulation in the main channel. Scale bar is 300 µm.

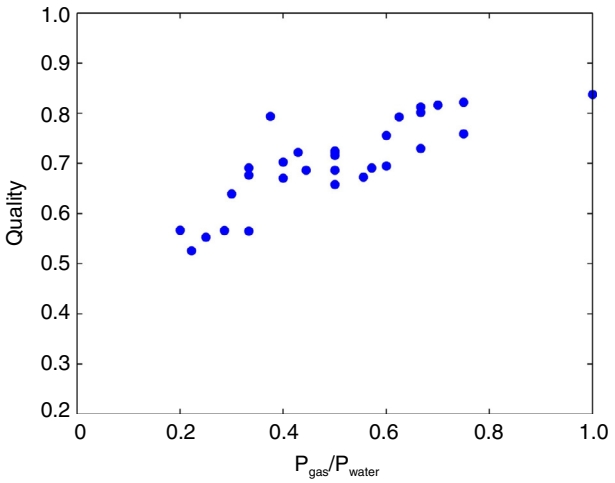

Figure 11

Foam quality in the main central channel next to the outlet.

flow in this "comb" geometry the next step is to quantify the type of flow in the lateral channels.

In case of foam flow, the flow through the comb sides channels is much more important than expected with simple Newtonian phase. Indeed due to the higher hydrodynamic resistance in the small lateral channels a Newtonian fluid flows preferentially in the larger channel. Figure 10 illustrates this phenomenon: as water phase flows easily in the small channels compared to bubbles, bubbles tend to accumulate at the centre channel forming a dry foam as represented by its quality close to the outlet in Figure 11. The comb-like two permeabilities geometry acts like a filter for the liquid phase. As can be seen in Figure 11 for $P_{gas}/P_{water} < 0.6$, the foam quality before the main channel outlet is higher than the one just after the bubble formation (*Fig. 6*).

In order to quantify the diversion of part of the flow to the small lateral channels we compare the flow rate in the main channel Q_2 to the one in the secondary channels next to the outlet for different values of gas and water pressure during the stationary state. Thanks to symmetry arguments the flow rates in the two secondary channels are identical and called Q_3 (Q_1 corresponds to the flow rate just before the "comb"). We precise that the flow rate considered here is the foam flux (liquid and gas) calculated from the measured velocity of the bubbles. In Figure 12, we plotted the ratio Q_3/Q_2 as a function of P_{gas}/P_{water} characterizing the flow. For a biphasic flow the flow rate is higher in the secondary channel than in the main one and the ratio Q_3/Q_2 can reach a value higher than 2.5 for small value of P_{gas}/P_{water}. Q_3/Q_2

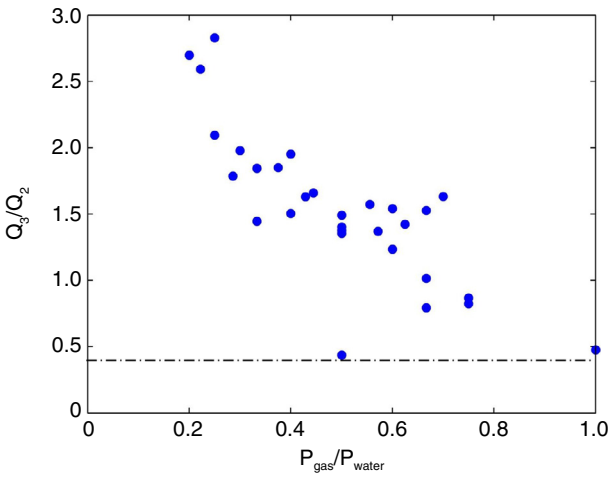

Figure 12

Flow rate ratio in the main and the secondary channels as a function of P_{gas}/P_{water}.

decreases with P_{gas}/P_{water} and tends to an asymptotical value equals to 0.4 which correspond to a Newtonian fluid flow as determined experimentally with our system using water and glycerol by PIV measurement (dashed line in *Fig. 12*). It is interesting to note that for biphasic flow with low value of P_{gas}/P_{water} all the bubbles are transported through the main channel and water goes preferentially in the small channels: starting for example with a foam quality of 0.15 for $P_{gas}/P_{water} = 0.3$, the quality in the main channel gets up to 0.6 at the outlet.

In these conditions Q_3/Q_2 is larger than for a Newtonian fluid. For high values of P_{gas}/P_{water} we observe a different regime where the quality of the foam in the main channel is close to the injected one and Q_3/Q_2 corresponds surprisingly to a Newtonian fluid. Characterization of the flows in the low permeabilities channels would help to get a complete understanding of the complex flow pattern behavior.

Even if observed without any oil, this observation brings clues to explain at least partly the mechanisms implied in EOR with foam, confirming in particular the interest of foam for fluid diversion in complex cases such as very heterogeneous formations or fractured reservoirs. A more detailed characterization of the phenomenon will be presented in a future article.

CONCLUSIONS

The high complexity of foam flow in real porous medium can be approached thanks to microfluidics tools, with very controlled quasi-2D flow confinement geometries. In this study, foam formation and transport properties were observed in microdevices. We studied two processes of foam formation, co-injection of water and gas illustrated by a phase diagram or fragmentation of large bubbles by a porous media and the flow of foam in a comb-like channel with a "two permeabilities" geometry. Those observations may be a basic illustration of some principles of EOR with foams. Perspectives of this work are the quantification of water and gas saturation in the microdevice channels as well as the study of the foam flow in presence of residual oil in order to improve foam physics understanding in porous media.

ACKNOWLEDGMENTS

Authors thanks Bernard Bourbiaux and Michel Robin (IFPEN) for fruitful discussions.

REFERENCES

1 Bernard G., Holm L.W. (1964) Effect of foam on permeability of porous media to gas, *SPE Journal* **4**, 3, 267-274.

2 Holm L.W. (1968) The mechanism of gas and liquid flow through porous media in the presence of foam, *SPE Journal* **8**, 4, 359-369.

3 Hanssen J.E., Holt T., Surguchev L.M. (1994) Foam Processes: An Assessment of Their Potential in North Sea Reservoirs Based on a Critical Evaluation of Current Field Experience, *SPE/DOE Improved Oil Recovery Symposium*, 17-20 April, Tulsa, Oklahoma.

4 Schramm L.L. (1994) *Foams: fundamentals and applications in the petroleum industry*, American Chemical Society.

5 Rossen W.R. (1996) Foams in enhanced oil recovery, *Surfactant Science Series*, 413-464.

6 Farajzadeh R., Andrianov A., Zitha P. (2010) Investigation of Immiscible and Miscible Foam for Enhancing Oil Recovery, *Industrial & Engineering Chemistry Research* **49**, 4, 1910-1919.

7 Hirasaki G., Miller C.A., Puerto M. (2011) Recent Advances in Surfactant EOR, *SPE Journal* **16**, 4, 889-907.

8 Farajzadeh R., Andrianov A., Krastev R., Hirasaki G., Rossen W. (2012) Foam-oil interaction in porous media: Implications for foam assisted enhanced oil recovery, *Advances in Colloid and Interface Science* **183**, 1-13.

9 Haugen A., Ferno M., Graue A., Bertin H. (2012) Experimental Study of Foam Flow in Fractured Oil-Wet Limestone for Enhanced Oil Recovery, *SPE Reservoir Evaluation & Engineering* **15**, 2, 218-228.

10 Singh G., Hirasaki G.J., Miller C.A. (1997) Dynamics of foam films in constricted pores, *AICHE Journal* **43**, 12, 3241-3252.

11 Marmottant P., Raven J.P. (2009) Microfluidics with foams, *Soft Matter* **5**, 18, 3385-3388.

12 Marchalot J., Lambert J., Cantat I., Tabeling P., Jullien M. C. (2008) 2D foam coarsening in a microfluidic system, EPL **83**, 64006.

13 Ma K., Liontas R., Conn C.A., Hirasaki G.J., Biswal S.L. (2012) Visualization of improved sweep with foam in heterogeneousporous media using microfluidics, *Soft Matter* **8**, 41, 10669-10675.

14 Duffy D.C., McDonald J.C., Schueller O.J.A., Whitesides G.M. (1998) Rapid prototyping of microfluidic systems in poly(dimethylsiloxane), *Analytical Chemistry* **70**, 23, 4974-4984

15 Ginn B.T., Steinbock O. (2003) Polymer surface modification using microwave-oven-generated plasma, *Langmuir* **19**, 19, 8117-8118.

16 Raven J.P., Marmottant P., Graner F. (2006) Dry microfoams: formation and flow in a confined channel, *Eur. Phys. J.* **51**, 137-143.

17 Lide D. (2011) *CRC Handbook of Chemistry and Physics*, CRC Press.

18 Garstecki P., Fuerstman M.J., Stone H.A., Whitesides G. M. (2006) Formation of droplets and bubbles in a microfluidic T-junction - scaling and mechanism of break-up, *Lab on A Chip* **6**, 3, 437-446.

19 Fu T., Funfschilling D., Ma Y., Li H. (2009) Scaling of formation of slug bubbles in microfluidic flow-focusing devices, *Microfluid Nanofluid* **8**, 467-475.

20 Stoffel M., Wahl S., Lorenceau E., Höhler R., Mercier B., Angelescu D.E. (2012) Bubble Production Mechanism in a Microfluidic Foam Generator, *Phys. Rev. Lett.* **108**, 198302.

21 Mason T.G., Wilking J.N., Meleson K., Chang C.B., Graves S.M. (2006) Nanoemulsions: formation, structure, and physical properties, *Journal of Physics-Condensed Matter* **18**, 41, R635-R666

22 Protière S., Bazant M.Z., Weitz D., Stone H.A. (2010) Droplet breakup in flow past an obstacle: A capillary instability due to permeability variations, *EPL* **92**, 54002.

23 Kim J.-U., Park B.H., Lee M.-H. (2013) Critical Parameters to Determine Mean Bubble Size of Generated Foams from a Foam Generator, *J. Appl. Polym. Sci.* **130**, 3, 2062-2067.

24 Fried A.N. (1961) The foam-drive process for increasing the recovery of oil, *Report of US Bureau of Mines*, BM-RI-5866.

25 Kovscek A.R., Bertin H.J. (2003) Foam mobility in heterogeneous porous media (I: Scaling concepts), *Transport in Porous Media* **57**, 17-35.

26 Kovscek A.R., Bertin H.J. (2003) Foam mobility in heterogeneous porous media (I: Experimental observations), *Transport in Porous Media* **57**, 37-49.

27 Prat L., Sarrazin F., Tasseli J., Marty A. (2006) Increasing and decreasing droplets velocity in microchannels, *Microfluidics and Nanofluidics* **2**, 3, 271-274.

Manuscript accepted in March 2014
Published online in June 2014